Dissertation

Development of a New Method to Estimate Ionospheric TEC Distribution by Single Frequency Measurements of GPS Signals

Graduate School of
Natural Science & Technology
Kanazawa University

Division of
Electrical Engineering and
Computer Science

Student ID No.: 1424042002
Name: WIN ZAW HEIN
Chief Advisor: Dr. Yoshitaka GOTO
Date of Submission: March 17, 2017

ACKNOWLEDGEMENT

Firstly, I deeply would like to express my sincere gratitude to my supervisor Dr. Yoshitaka GOTO who accepted me to do this research under his supervision and supported me valuable guidance, suggestions, explanations and motivation on my daily research, and useful lectures from the basic study to advanced technologies. His supervision made me to improve my current study and future profession.

I especially would like to be thankful to Professor Yoshiya KASAHARA who gave me an opportunity to participate in this research and laboratory, and gave me guidance, suggestions, and useful lectures. Those are really helpful to my research.

I would like to express my appreciation and thanks to Professor Satoshi YAGITANI who kindly gave me useful guidance, suggestions, lectures and beneficial comments to my research.

I also would like to be grateful to Dr. Mitsunori OZAKI who gave useful lectures, experiments to my research and valuable suggestions and comments in my research, and also Dr. Tomohiko IMACHI who gave useful lectures and experiments to my research.

I would like to be thankful to Dr. Akihiro HIRANO who gave valuable suggestions, guidance and comments to my research.

I would like to be grateful to Professor Yoshihiko UESUGI who connected me with Kanazawa University and gave me a lot of useful information, suggestions and supported study field trips.

I also would like to thank to Professor Masato MIYOSHI who gave me useful lectures and Dr. Yoshihiro TAKADA who was involved in our laboratory and gave me suggestions and comments.

I specially would like to be thankful to my tutor friend, Mr. Yusuke KASHIWA who was involved and helped me a lot in my experimental works and everything in my daily life in Kanazawa and also to Dr. Shoya MATSUDA who helped me a lot in my daily life.

I also would like to thank Mr. Atsushi MATSUI who was involved in our research group and helped me with my experimental work a lot, and Mr. Mamoru OTA who helped and suggested me in programming and accessing the network, and also Mr. Hiroki OKUDA, Mr. Yuji TANAKA and Mr. I Made Agus Dwi Suarjaya

(from Indonesia) who were involved and helped me useful information in our laboratory and daily life.

Many thanks to all my laboratory members who helped me in my research, gave me useful information and solved every problem in my daily life.

I especially would like to acknowledge to Mr. Tomoki NITTA (Director General of JICA Hokuriku), Mr. Toru SAITO (Deputy Director, Program Division), Ms. Yukari HIRATA (Program Officer), Ms. Airi FUKUSHIMA (Supporting staff), Ms. Tsutayo KIMIZU (Staff), and all staffs who work at JICA (Japan International Corporation Agency) Hokuriku and Myanmar Branch, and also JICA who supported me scholarship for daily allowance and educational requirements.

The code pseudorange data used in this study were provided by Geospatial Information Authority of Japan. The ionospheric vertical TEC map and the orbital data of the GPS satellites were provided by the International GNSS Service (IGS). Therefore, I would like to thank them for supporting data archive to my research.

I would like to acknowledge to our Ministry (Ministry of Science and Technology) and EEHE (Enhancement of Engineering Higher Education) project in Myanmar, and the Technical Cooperation Board of EEHE project who selected and permitted me to go and study in Japan.

Finally, I deeply would like to be thankful to my dear father, mother and my family who love never ceases to amaze me and gave a change to study in Japan. Words cannot be expressed how grateful I am to my parents and family for all of the sacrifices that they’ve made on my behalf.

TABLE OF CONTENTS

Pages

LIST OF FIGURES

CHAPTER 1
INTRODUCTION

1.1 Background of Research

The Earth's ionosphere is composed of ions and electrons which are the result of ionization of neutral particles due to solar ultraviolet radiation. These charged particles are called plasma. An important feature of the ionospheric plasma in terms of radio waves is its ability to reflect and delay radio waves. The ionosphere is divided into several layers; D, E, F1, and F2 layers according to altitude distribution of electron density. Figure 1.1 shows typical electron density distribution in altitude for daytime and nighttime. The distributions are calculated by the International Reference Ionosphere (IRI) model [1]. In the figure, horizontal axis shows electron density and vertical axis does altitude. The blue solid line and dotted line show electron density profiles in daytime and nighttime, respectively. The red, green and magenta lines show maximum values of electron density of F2, E, and D layers, respectively. In the profile, there is no F1 peak. Each layer has critical frequency which is the limitation of frequency whether radio wave can pass through the layer or not, as shown in Figure 1.2. This frequency is called plasma frequency and is calculated by f_{p} [kHz] $\cong 8.98 \times \sqrt{n\ [/\mathrm{cm}^3]}$ where n is electron density. The lowest critical frequency is found in the D layer and it increases to the F2 layer. The highest plasma frequency is found in the F2 layer called f_0F_2.

In satellite communications, the frequency of radio waves has to be much higher than f_0F_2 to pass through the ionosphere. Radio waves whose frequency is lower than f_0F_2 are reflected. Even if the frequency is much higher than f_0F_2, the ionospheric plasma causes delay in radio wave propagations between satellites and the ground. The delay is proportional to the total electron content (TEC) which denotes integration of electron density along the signal propagation path. The amount of the delay, for example, varies up to several tens of nanoseconds in the Global Positioning System (GPS) signals. Drastic changes of ionospheric plasma density sometimes cause short-period fluctuations of amplitude of received signals, which is

called scintillation.

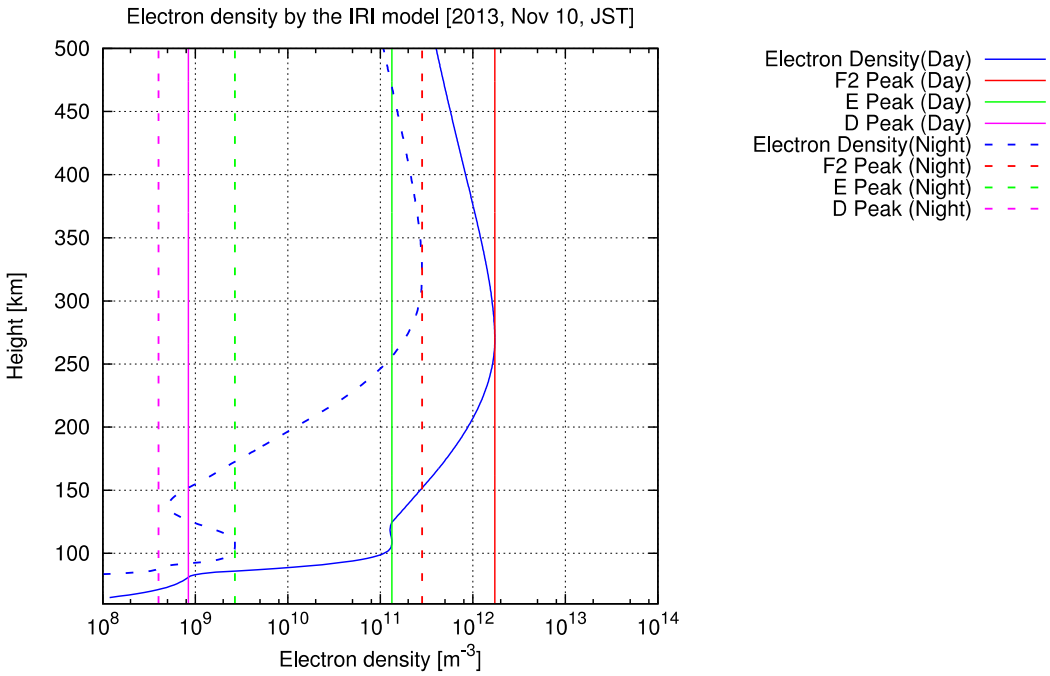

Figure 1.1 Typical electron density profiles in altitude for daytime and nighttime which are calculated by the International Reference Ionosphere model.

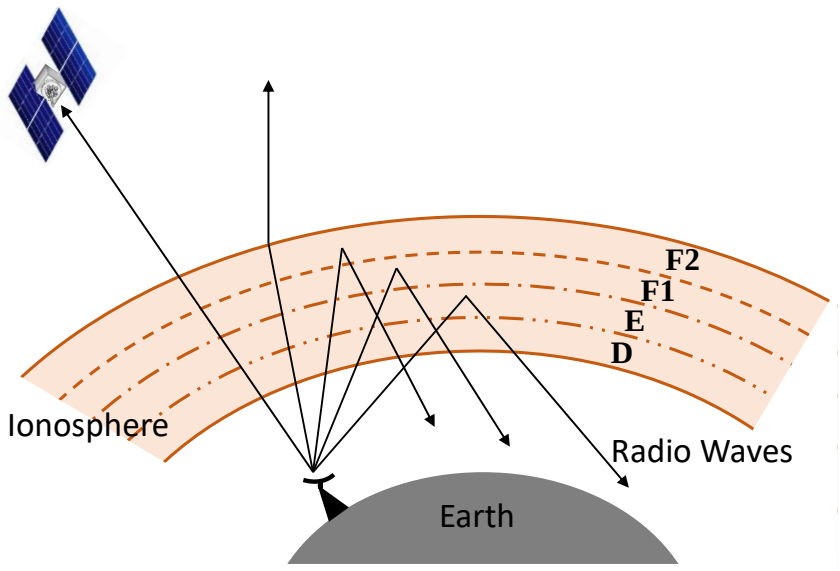

Figure 1.2 Schematic chart of reflection and penetration of radio waves in the ionosphere.

Monitoring of the ionospheric plasma has getting more important with the expansion of use of the space. The ionospheric plasma density distribution has been investigated by radar observations from the ground and direct observations from spacecraft. Sounding observations from the ground were the most general method to probe ionospheric density in the past century. A density profile in the lower ionosphere is obtained from frequency dependence of radar echoes. In-situ electron density observation in the ionosphere from spacecraft is achieved by several ways; measurement of UHR frequency of plasma waves, impedance probe experiment and so on. In these radar and in-situ measurements, there are restrictions in observational periods, regions or time continuity. These restrictions are essential problems in a view point of continuous monitoring of the ionospheric electron density distribution because its variation is not so simple that it can be estimated by an empirical model. The continuous monitoring of the total electron content (TEC) using observational networks of GNSS (Global Navigation Satellite System) signals has recently become popular in many countries/regions, such as Japan, United States, Europe and New Zealand. In Japan, more than 1,200 GNSS stations are installed all over the islands. This observational network is called GEONET [2] and was originally built for land survey. This kind of GNSS observation networks make it possible to reconstruct vertical TEC maps in wide regions in high spatial and temporal resolutions and are now used as an important information source of space weather forecast. Most of the networks are, however, built in mid latitude regions. It is important to expand the observation network in low latitude regions where interesting phenomena with drastic density variations occurs, such as plasma bubble.

In the GNSS observation stations, multi-frequency receivers are generally installed. They make it possible to estimate the ionospheric effects accurately because only the ionospheric delay depends on the frequency among ranging errors. The multi-frequency receivers used in the GNSS stations are, however, much more expensive than single frequency receivers which are widely distributed as consumer products. In order to expand the TEC observation networks, it is expected that the single frequency receivers can be used for the TEC measurements. In this study, this issue was addressed.

1.2 Reconstruction Methods of Ionospheric Vertical TEC Distribution

There are several methods which are used for reconstruction of wide regions of TEC map from slant TECs measured by GNSS signals. Global ionosphere maps (GIM) have been developed as snapshots of the global ionospheric TEC by several research institutes, such as CODE (Center for Orbit Determination in Europe), ESOC/ESA (European Space Operations Center from European Space Agency) and JPL (NASA Jet Propulsion Laboratory) [3, 4]. The GIMs are based on slant TECs obtained from dual frequency measurements at GNSS stations all over the world. For the reconstructions of ionosphere maps, single-layer models are assumed and spherical harmonics are used to interpolate the observed TEC values. The GIMs produced by Code with international GNSS service (IGS) are provided every hour every day as IONEX that is a common exchange format which represents the ionosphere map [5].

The purpose of this study is to develop a method to estimate local TEC map from single frequency measurements. Figure 1.3 shows a concept chart of ionospheric TEC estimation from single frequency GNSS signals. The TEC map is estimated on the assumption of thin layer ionosphere under the condition that receiver location is accurately known. Because the receiver clock error is unknown as well as the ionospheric delay, the problem is how to separate them by spatial distribution of the TEC and slant factor. In that sense, the problem is much more difficult than the map reconstructions using the dual frequency measurements which are introduced above.

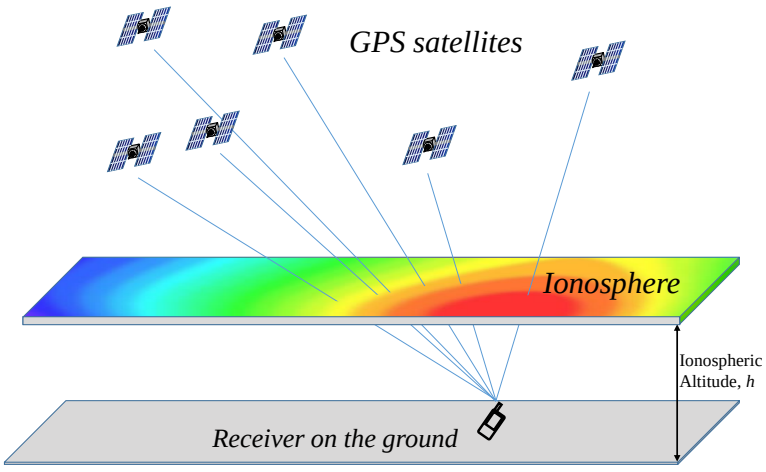

Figure 1.3 Concept chart of ionospheric TEC observation using GNSS signal.

1.3 Contribution to the Present Study

In previous experimental works to observe ionospheric TEC, multiple frequency receivers were used. However, they are not easy to obtain for researchers because of cost or budget problems. Development of a method for ionospheric TEC estimation from single frequency measurements of GNSS signals makes it possible for researchers in the low latitude region countries such as Southeast Asian countries where the GNSS stations are not yet constructed to conduct experimental and practical works. It is important to conduct such practical works on the ionosphere in the fields of radio engineering, such as satellite communications and long distance communications using HF bands as well as in the field of space science.

CHAPTER 2
FUNDAMENTAL TECHNIQUES OF GPS SIGNAL PROCESSING AND DATA

2.1 Global Positioning System (GPS)

The GPS is one of the most popular global navigation satellite system (GNSS) that provides location and precise time in all weather conditions anytime and anywhere all over the world. The fundamental technique of GPS positioning is based on a triangulation method. Ranges between a receiver and several simultaneously observed satellites are measured from propagation time of signals. Orbits of the satellites are forecasted and broadcasted along with the GPS signal to the user. Through several known positions of the satellites and the measured distances between the receiver and the satellites which are called pseudorange, the position of the receiver is determined. During this process, accurate time is also obtained.

The GPS constellation consists of 31 satellites in six orbital planes with more than four satellites in each plane. The ascending nodes of the orbital planes are equally spaced by 60 degrees [6]. The inclination angles of the orbital planes are 55 degrees. Then, distribution of the satellites in the sky depends on the latitude where the receiver is set. Each GPS satellite is in a nearly circular orbit with a semi-major axis of 26,578 km and a period of about twelve hours. The orbits are arranged so that at least six satellites are always visible from everywhere on Earth's surface.

Each GPS satellite transmits plural navigation messages. The navigation message used for Standard Positioning Service (SPS) contains orbital information of the satellites which are called ephemeris and almanac, and error correction parameters for ionospheric delay and satellite clock error [7]. The message is modulated by pseudorandom noise code called Coarse-Acquisition (C/A) code. The C/A code is allocated to each satellite independently. The carrier frequency of the modulated message is 1575.42 MHz in the SPS.

The basic GPS observables are code pseudoranges and carrier phases. In this study, only code pseudoranges are used. The pseudorange is the pseudo distance

between the satellite and the receiver which is derived from propagation time of the signal. The propagation time is estimated through maximum correlation analysis between the measured signal and replica signal which is a C/A code generated in the GPS receiver. The measured pseudorange is different from the geometric distance between the satellite and the receiver because it includes errors of both clocks of the satellite and receiver and influences of the signal transmitting mediums, such as ionosphere and troposphere. The precision of the pseudorange measurements depends on the electronic abilities.

2.2 Propagation Characteristic of GPS Signal

Every transmission signal is affected by the medium through which it travels from the transmitter to the receiver. The propagation medium changes velocity and direction of the signals, which is called refraction. Since the GPS orbits are located at an altitude of about 20,200 km, the GPS signals pass through the Earth's atmosphere from the satellites to the receivers. The travel distance depends on the elevation angle of satellite.

The refractive index of a medium denoted as *n* can be defined by

$$n = \frac{c}{v}, \tag{2.1}$$

where *c* is the speed of light and *v* is signal speed in the medium [8]. The atmospheric refractive index of GPS signal generally refers to the ionosphere and troposphere. The refractive index of ionosphere and troposphere are not uniform along the signal path from the satellite to the receiver. Then, the propagation time is proportional to the integration of the refractive index along the propagation path;

$$\tau = \frac{1}{c}\int_s^r n(l)dl, \tag{2.2}$$

where τ is the propagation time, *s* and *r* are indicated satellite and receiver. Then, the propagation delay $\Delta\tau$ of the signal due to refraction can be defined as

$$\Delta\tau = \frac{1}{c}\int_s^r [n(l) - 1]dl. \tag{2.3}$$

When the refractive index of medium has a frequency dependence of the signal, this medium is called dispersive medium. When the signal passes through the dispersive medium, the phase velocities and group velocities of signals are different. From Eq. (2.1), the phase refractive index and group refractive index can be defined as follows

$$n_p = \frac{c}{v_p}, \tag{2.4}$$

$$n_g = \frac{c}{v_g}, \tag{2.5}$$

where v_p is phase velocity and $v_g$is group velocity. In a vacuum, the phase velocity and group velocity are same. The relationship between phase refractive index and group refractive index is defined as

$$n_g = n_p + f\frac{dn_p}{df}. \tag{2.6}$$

From this basic calculation process of propagation delay, ionospheric delay can be determined.

2.2.1 Ionospheric Delay

As the satellites signals pass through the ionosphere, the propagation of signals is affected, which is called ionospheric delay. This effect is an important error source in GPS positioning. The propagation delay time of signal depends on the integration of electron density along the propagation path because refractive index is related to the electron density in the ionosphere. The integration is called total electron content (TEC). The TEC along the propagation path from the satellite to the receiver is called slant TEC and it is defined as,

$$I_{\text{slant}} = \int_s^r N_e dl, \tag{2.7}$$

where N_e is the electron density. The relationship between refractive index and electron density can be defined by

$$n_p \cong 1 - \frac{e^2 N_e}{8\pi^2 m\varepsilon_0 f^2}, \tag{2.8}$$

where *e*, *m*, ε_0 and *f* are charge and mass of the electron, permittivity of free space and the signal frequency, respectively. From this equation, the phase delay $\Delta\tau_p$ of the signal which passes through the ionosphere can be calculated as follows,

$$\Delta\tau_p = \frac{1}{c}\int_s^r [n_p(l) - 1]dl, \tag{2.9}$$

$$= -\frac{1}{c}\int \frac{e^2 N_e}{8\pi^2 m\varepsilon_0 f^2} dl,$$

$$\Delta\tau_p = -\frac{e^2}{8\pi^2 m\varepsilon_0 c f^2} I_{\text{slant}}. \tag{2.10}$$

From Eq. (2.6), the group refractive index and group delay is represented as

$$n_g = 1 + \frac{e^2 N_e}{8\pi^2 m\varepsilon_0 f^2}, \tag{2.11}$$

$$\delta_{\text{ion}}^i = \frac{e^2}{8\pi^2 m\varepsilon_0 f^2} I_{\text{slant}}. \tag{2.12}$$

Generally, the ionospheric delay is measured by dual frequencies L1 and L2 of GPS signals because only ionospheric delay depends on the signal frequency among the measurement errors. The ionospheric group delay of L1 signal is calculated by

$$I_{\text{L1}} = \frac{{f_{\text{L2}}}^2}{({f_{\text{L1}}}^2 - {f_{\text{L2}}}^2)} (\rho_{\text{L2}} - \rho_{\text{L1}}), \tag{2.13}$$

where f_{L1} and f_{L2} are the frequencies at L1 and L2 signals. ρ_{L1} and ρ_{L2} are the code pseudoranges at L1 and L2 signals. From ionospheric group delay in Eq. (2.12), the total electron content (TEC) can be determined by

$$I_{\text{slant}} = \frac{8\pi^2 m\varepsilon_0}{e^2} \frac{{f_{\text{L1}}}^2 {f_{\text{L2}}}^2}{({f_{\text{L1}}}^2 - {f_{\text{L2}}}^2)} (\rho_{\text{L2}} - \rho_{\text{L1}}), \tag{2.14}$$

where I_{slant} is the slant TEC along the propagation path from the satellite to the receiver. The ionospheric TEC is generally represented in TEC Units (TECU), defined as 10^{16} electrons/m^2.

In the dual frequency measurements, there are hardware effects called differential code bias (DCB). The DCB is caused by different of signal transmission speed in receiver and transmitter between different codes and frequencies. The measured ionospheric delay includes these effects. The DCB varies with outside environment such as temperature. In order to obtain the accurate TEC in the dual frequency measurements, the effect of the DCB has to be removed from the TEC measurements.

2.3 Coordinate System

The coordinate systems concerned with this study are described in this section.

2.3.1 ECEF (Earth-Centered Earth-Fixed) Coordinate System

The ECEF coordinate system is a right-handed Cartesian system (*x*, *y*, *z*) and *x*-axis is in the direction from the intersection of the Greenwich Meridian called zero-meridian, *z*-axis is in the direction to the north pole of the Earth's axis with Earth's rotation, and *y*-axis is in the direction of right-handed orthogonal to *x*-axis and *z*-axis. The origin is the center of the Earth and *x*-*y* plane is defined as the equatorial plane of the Earth. The coordinate is fixed with Earth's rotation and used to describe the location of the satellites and receivers in this study.

2.3.2 Earth-Centered Inertial Coordinate System (ECI)

The Earth-Centered Inertial (ECI) coordinate is used to describe the motion of satellites. The origin of the system is defined at the center of the Earth. The ECI coordinate system uses the right-handed Earth-center inertial system as ECEF and the rotation of terrestrial object is fixed with Earth's rotation in order to face to the Earth surface to represent their positions and velocities in latitude, longitude and altitude. The rotation of terrestrial objects in space is simplified as non-rotation frame in the equation of ECI coordinate system. Therefore, ECI frame is useful for specifying the

direction toward celestial objects from Earth surface with regardless of rotation. In this study, ECI coordinate system is used to define satellite position and this position is changed to the ECEF coordinate when the position is measured from the Earth. A location vector defined in the ECI coordinate system can be transformed into that in ECEF coordinate system, and vice versa [6].

2.4 Ionospheric Pierce Points

The ionospheric delay is caused by the total electron content (TEC) in the ionosphere along the signal propagation path from the satellite to the receiver. Since the electron density is concentrated at F2 layer in the ionosphere, a thin layer model is generally assumed to represent the ionospheric density distribution. The intersection point between the ionospheric thin layer and the signal propagation path is called the ionospheric pierce point (IPP) as shown in Figure 2.1.

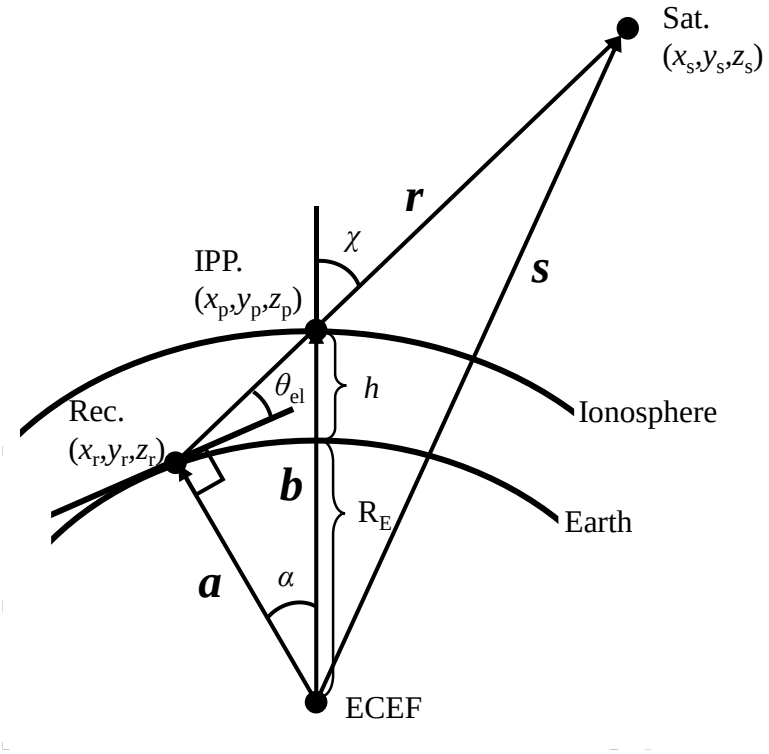

Figure 2.1 Ionospheric pierce point and its vector expression.

The figure shows ionospheric pierce point (IPP) and its vector expression where ***a***, ***b*** and ***s*** show location vectors of the receiver, IPP, satellite in the ECEF

coordinate system respectively. The vector $\boldsymbol{r}$ is the receiver-to-satellite vector. The IPP vector can be represented by using these vectors as follows,

$$\boldsymbol{b} = \boldsymbol{a} + \gamma \boldsymbol{r}, \tag{2.15}$$

where γ is an index at IPP. When the ionospheric altitude h is given, that is $|\boldsymbol{b}|$ is known, γ can be calculated as follows;

$$\gamma = \frac{|\boldsymbol{b}||\boldsymbol{r}| - \boldsymbol{a}\cdot\boldsymbol{r}}{|\boldsymbol{r}|^2}. \tag{2.16}$$

2.5 Least Squares Method

Least squares method is a method to fit the data using ideal data expression in linear term for the model and to realize unknown error to the model. This model can be used to predict unobserved values by summarizing the known data sets from the same system. Linear least squares is the parameters fitting method to get approximated parameters in an overdetermined system of the linear equations. The approximation in linear least square can be defined by using the minimization of the sum of squared differences between the data values and their corresponded values. The best fitting is occurred when minimization becomes zero. However, it is impossible that the minimization becomes zero in numerically and the measured minimization value is defined as error of the least square fitting.

When the matrix $\boldsymbol{A}$ and vector $\boldsymbol{b}$ is given, the following equation can be solved by the linear least squares method;

$$\boldsymbol{A}\boldsymbol{x} = \boldsymbol{b}. \tag{2.33}$$

In the calculation, the size of $\boldsymbol{x}$ has to be less than the size of $\boldsymbol{b}$. the solution vector is represented by

$$(\boldsymbol{A}^T\boldsymbol{A})\boldsymbol{x} = \boldsymbol{A}^T\boldsymbol{b}. \tag{2.34}$$

2.6 GPS Data Obtained by GEONET and IGS

In this study, we used GPS data obtained by the GEONET (GNSS Earth Observation Network System) in Japan and also the IGS stations. The GEONET was built by the Geographical Survey Institute (GSI) in Japan [2]. It is originally built for land survey and consists of approximately 1200 GNSS observation stations all over Japanese island, as shown in Figure 2.2. All the stations are installed in average spacing 25-30km between two neighbor stations. All the receivers in the network are multiple frequency type.

Data obtained by the receivers are provided as RINEX (Receiver INdependent EXchange) format. The RINEX is a common text format that users can use commonly regardless of the type of receiver. The RINEX data includes observation data, navigation data, and so on. The observation data include information of code pseudoranges, carrier phase, observed signal strength. The data are available every 30 seconds.

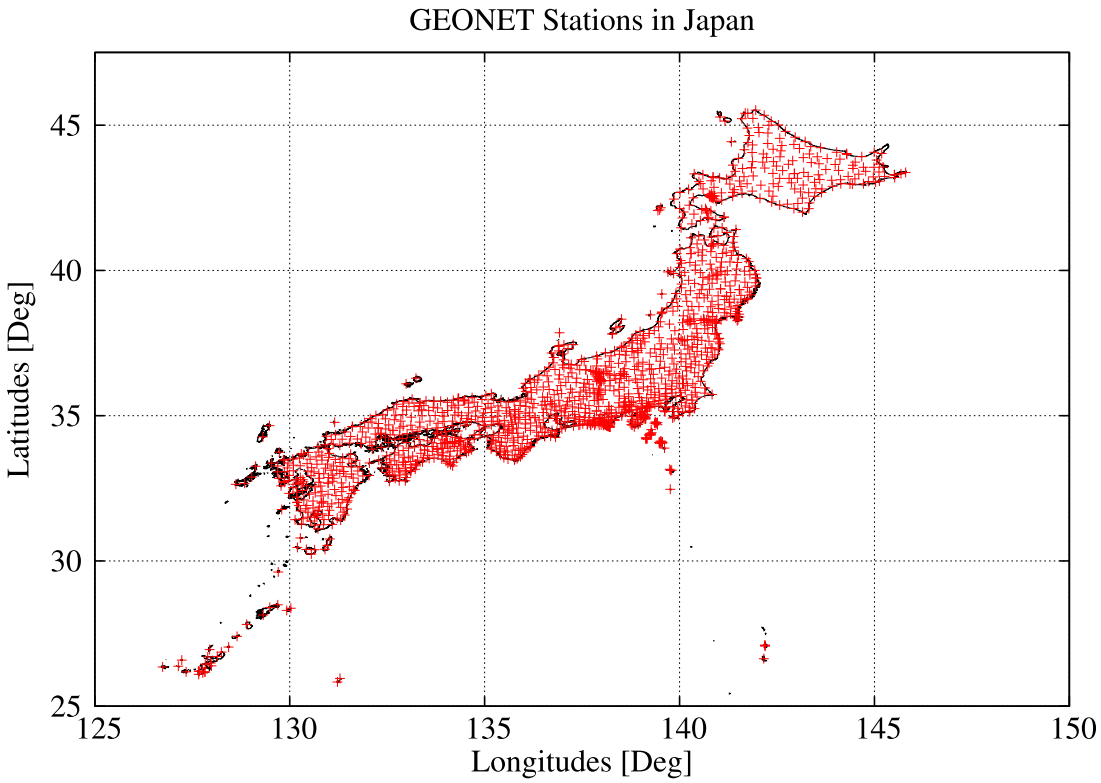

Figure 2.2 The locations of GEONET stations in Japan.

The NASA Jet Propulsion Laboratory (JPL) provides global ionospheric map (GIM) with every 2 hours from data obtained at more than 400 GNSS stations all over the world. They support global TEC maps with resolution of 5º x2.5º at longitudinal and latitudinal variation. These maps are driven by dual frequency measurements of GNSS signals and it can be used as reference of our results.

CHAPTER 3

ESTIMATION METHOD OF IONOSPHERIC TEC USING SINGLE FREQEUNCY GPS SIGNALS

In this chapter, a new estimation method of ionospheric TEC distribution from single frequency GPS measurements is described.

3.1 Single Frequency Measurements

3.1.1 Errors in Code Pseudoranges

The basic GPS observables are code pseudoranges and carrier pseudorange. In this study, code pseudoranges are used. The principle of the GPS measurements and their mathematical expressions of code pseudoranges are described in this section.

The pseudorange is a measured distance between the satellite and receiver which is derived from propagation time of the signal. The propagation time is estimated through maximum correlation analysis between the measured C/A code on the L1 signal and replica signal generated in the GPS receiver. The pseudorange is different from the geometric distance between the satellite and the receiver because of both satellite clock error and receiver clock error, and influences of the signal transmitting mediums of ionosphere and troposphere. Figure 3.1 shows relation between geometric distance and pseudorange distance with the errors.

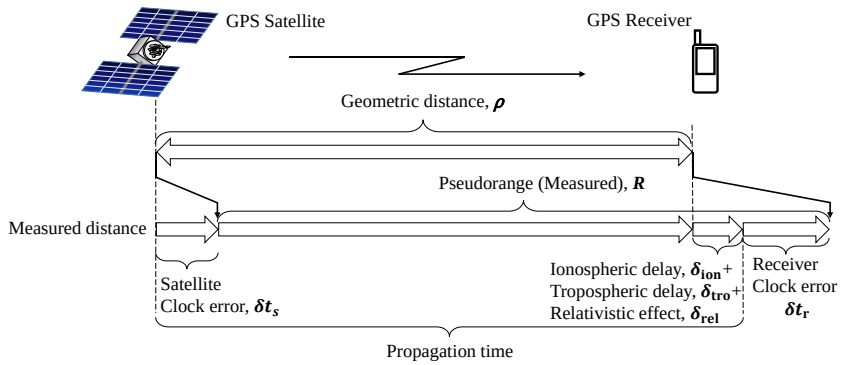

Figure 3.1 Relation between geometric distance and pseudorange with errors.

The signal transmission time of the satellite is denoted by t_s, and the reception time of the receiver is denoted by t_r. In case of vacuum medium and error-free situation, the measured pseudorange $R = (t_r - t_s)c$ is equal to the geometric distance $\rho = \sqrt{(x_s - x_r)^2 + (y_s - y_r)^2 + (z_s - z_r)^2}$ where (x_s, y_s, z_s) is the satellite location at time t_s and (x_r, y_r, z_r) is the receiver location at time t_r in the ECEF coordinate system. Actually, we need to take errors in the pseudorange, such as ionospheric effects, tropospheric effects, Earth tide effects, multipath and relativistic effects, into account and then the relation between the pseudorange and geometric distance is represented by

$$R = \rho + c(\delta t_r - \delta t_s) + \delta_{ion} + \delta_{tro} + \delta_{mul} + \delta_{rel} + \varepsilon. \quad (3.1)$$

The measured pseudorange equals to the geometric distance ρ between the satellite at the transmission time error δt_s and the reception time error δt_r with plus or minus several error corrections. δ_{ion} and δ_{tro} denote the ionospheric and tropospheric effects along the propagation paths of the signal. δ_{mul} denotes the multipath effects, and δ_{rel} denotes the relativistic effects. The residual errors are denoted by ε.

In the present study, we propose a method to estimate TEC map from δ_{ion} in Eq. (3.1). Since the receiver clock error δt_r is also unknown, a spatial model for vertical TEC distribution is assumed to separate the effects of δ_{ion} and δt_r. In this study, multipath effect δ_{mul} and other bias effect such as Earth tide effects are neglected.

3.1.2 Correction of Satellite Position and Clock Errors

The international GNSS service (IGS) provides precise ephemeris data to obtain accurate satellite orbits and clock error corrections [9]. The IGS supports three types of precise ephemeris data: ultra-rapid, rapid and final ephemeris. The ultra-rapid can be used for real time observation, and rapid and final ephemeris can be used for analysis of archive data. In this study, final ephemeris is used. Accuracy of final ephemeris for satellite orbits and clock error correction is less than 2.5 cm and 20 psec in RMS [9]. The data are provided every 5 minutes interval and thus we interpolate them with Lagrange polynomial function. To construct a polynomial of degree *n*

passing through n+1 data points of $(x_0, y_0), (x_1, y_1), \ldots, (x_n, y_n)$, the Lagrange polynomial function is represented by

$$P_n(x) = \sum_{i=0}^{n} y_i l_i(x),$$

$$l_i(x) = \prod_{j=0, j\neq i}^{n} \frac{(x-x_j)}{(x_i-x_j)}. \tag{3.2}$$

In this study, we adopt 9th order polynomial function, and the accuracy of the satellite locations (x_s, y_s, z_s) and clock error effects δt_s after interpolation are a few centimeters in RMS.

3.1.3 Estimation of Relativistic Effect from Precise Ephemeris

According to the relativity theory, there is a time difference between the satellite velocity and receiver velocity. To obtain accurate clock error, relativistic effects should be taken into account. The relativistic effect can be expressed as

$$\delta_{\text{rel}} = -\frac{2\boldsymbol{u}\cdot\boldsymbol{v}}{c^2}, \tag{3.3}$$

where $\boldsymbol{u}$ and $\boldsymbol{v}$ are the position and velocity of the satellite in the ECI coordinate system respectively [10].

3.1.4 Estimation of Satellite Antenna Offset

The satellite antenna phase center is taken into account because we use precise ephemeris which denotes locations of the satellite body center. The phase difference between satellite body center and antenna is called satellite antenna offset, as shown in Figure 3.2. In the figure, $\boldsymbol{R}_{\text{sun}}$, is a vector to Sun direction and $\boldsymbol{z}$ is a vector to the Earth direction and it is same as antenna direction. $\boldsymbol{x}$ and $\boldsymbol{y}$ are vectors to the horizontal plane of the satellite. The antenna offset error causes errors in GPS ranging from a few millimeter to centimeter accuracy.

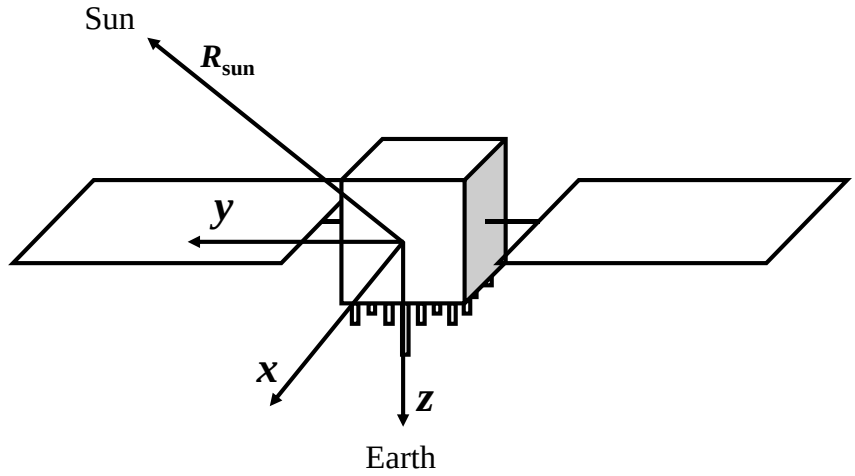

Figure 3.2 Satellite coordinate system whose origin is satellite body center.

The distance from the satellite body center to the antenna center is estimated by

$$\boldsymbol{s}^p = \boldsymbol{s}_0{}^p + \boldsymbol{E}_{\text{Sat-to-ECEF}}\Delta\boldsymbol{s}^p, \tag{3.4}$$

where $\boldsymbol{s}_0{}^p$and $\boldsymbol{s}^p$ are satellite body center and antenna center in the ECEF. $\Delta\boldsymbol{s}^p$is the antenna offset in the satellite coordinate system shown in Figure 3.2. $\Delta\boldsymbol{s}^p$is specific for satellite type. $\boldsymbol{E}_{\text{Sat-to-ECEF}}$ is a conversion matrix from the satellite coordinate system to the ECEF which is represented by

$$\boldsymbol{E}_{\text{sat-to-ECEF}} = \begin{pmatrix} e_x \\ e_y \\ e_z \end{pmatrix}, \tag{3.5}$$

where

$$e_z = \frac{\boldsymbol{s}_0{}^p}{\|\boldsymbol{s}_0{}^p\|}, \tag{3.6}$$

$$e_y = \frac{e_z \times e_s}{\|e_z \times e_s\|}, \tag{3.7}$$

$$e_s = \frac{\boldsymbol{R}_{\text{sun}} - \boldsymbol{s}_0{}^p}{\|\boldsymbol{R}_{\text{sun}} - \boldsymbol{s}_0{}^p\|}, \tag{3.8}$$

$$e_x = e_y \times e_z. \tag{3.9}$$

3.1.5 Tropospheric Delay

Since the GPS signals pass through the lower atmosphere above the Earth called troposphere, the signals are affected by composition of water vapor and dry gases such as N_2 and O_2 in this region. The altitude of water vapor in troposphere is about below 12 km and the altitude of dry gases is, however, up to hundred kilometers and almost three-quarter of dry gases are found in troposphere [8]. This water vapor and dry gases affect to the GPS signals along the propagation path. As the refractive index of the troposphere does not depend on the frequency of the signal in GPS, the troposphere is non-dispersive medium for GPS signals and the group velocity and phase velocity are same in the troposphere. Therefore, all carrier frequencies of GPS signals have common delay and the tropospheric delay cannot be estimated by dual frequency measurement of GPS signals. The tropospheric delay is generally 2.5 to 25 meters depending on the elevation angle of satellites as shown in Figure 3.3. In this study, we estimate the tropospheric delay by Hopfield model [8].

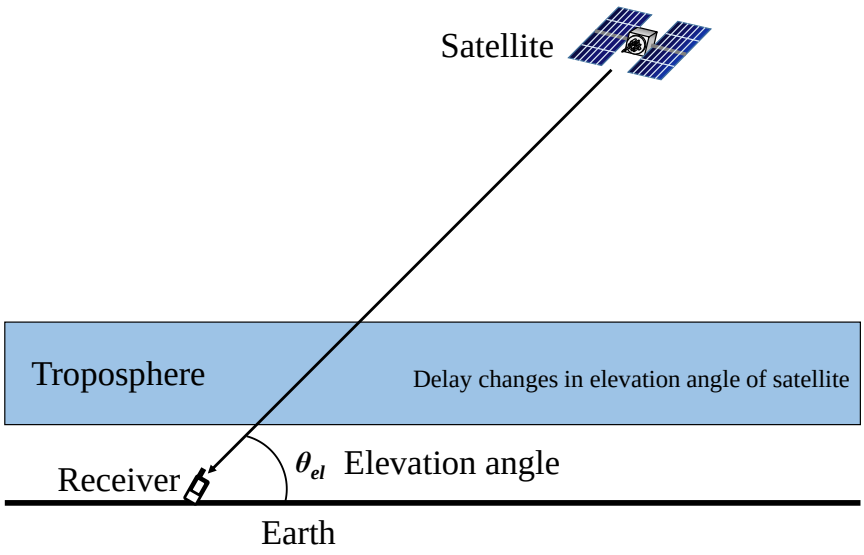

Figure 3.3 Tropospheric delay and elevation angle dependence.

In Hopfield model, the refractivity profile of dry delay is represented by

$$n_d(h) = n_{d0}\left(1 - \frac{h}{h_d}\right)^4, \tag{3.10}$$

where h is the height of the receiver above the sea level, n_{d0} is the dry refractive index at surface, and h_d is the altitude where the dry refractivity is zero which is assumed as 43 km. The refractivity profile of wet delay is defined same as dry delay as follows,

$$n_w(h) = n_{w0}\left(1 - \frac{h}{h_w}\right)^4, \tag{3.11}$$

where n_{w0} is the wet refractivity at surface of the Earth and h_w is the altitude that the wet refractivity equals to zero and it is assumed to be 12 km.

The total tropospheric delay along the propagation path is defined by

$$\delta_{\text{tro}} = \int [n_d(h) + n_w(h)]dh, \tag{3.12}$$

$$\cong n_{d0}h_d + n_{w0}h_w, \tag{3.13}$$

$$\cong \delta_{\text{tro}}^{\text{dry}} + \delta_{\text{tro}}^{\text{wet}}, \tag{3.14}$$

where $\delta_{\text{tro}}^{\text{dry}}$ and $\delta_{\text{tro}}^{\text{wet}}$ are delays due to dry and wet refractivities, respectively. These delays in meter can be calculated by

$$\delta_{\text{tro}}^{\text{dry}} = 77.6 \times 10^{-6} \frac{P_0}{T_0} \frac{h_d}{5} \text{[m]}, \tag{3.15}$$

$$\delta_{\text{tro}}^{\text{wet}} = 0.373 \times 10^{-6} \frac{e_0}{{T_0}^2} \frac{h_w}{5} \text{[m]}, \tag{3.16}$$

where P_0 [hPa] is the total pressure, e_0 [hPa] is partial pressure of water vapor, and T_0 is temperature in Kelvin.

The above-mentioned tropospheric delay is converted to slant delay depending on elevation angle of the signal path by using a mapping function as follows;

$$\delta_{\text{tro}} = (\delta_{\text{tro}}^{\text{dry}} + \delta_{\text{tro}}^{\text{wet}}) \frac{1}{\sin(\theta_{\text{el}})}. \tag{3.17}$$

This delay model is used in this study to estimate the tropospheric delay. The tropospheric dry delay which affects to the GPS signals is about 2.3-2.6 meter in

zenith direction at sea level before correction. Among this two dry delay and wet delay, dry delay highly affects to the GPS signals. The wet delay depends on the composition of water vapor and its accuracy is about 1-2 cm based on the meteorological conditions. After using Hopfield model, the tropospheric delay can be corrected with accuracy of 5-10 cm [8].

3.2 Estimation Model of Ionospheric TEC

As described in 2.2.1, the ionospheric delay δ_{ion} is directly proportional to the total electron content (TEC). This TEC is called slant TEC. Defining the slant TEC from the i^{th} satellite to the receiver by I^i_{slant} and $\frac{1}{\Lambda} \equiv \frac{e^2}{8\pi^2 m\varepsilon_0 f^2}$, Eq. (2.12) can be represented as the following formula,

$$\delta^i_{\text{ion}} = \frac{I^i_{\text{slant}}}{\Lambda}. \tag{3.18}$$

In this study, we estimate I^i_{slant} from single frequency measurement of GPS signals by adopting a spatial model for vertical TEC distribution in the ionosphere, as describe as before.

Under the condition that the receiver location (x_{r}, y_{r}, z_{r}) is accurately known, R, ρ, δt_{s}, δ_{tro} and δ_{rel} in Eq. (3.1) can be estimated as described in previous sections. Then, only δ^i_{ion} and δt_{r} are undetermined. While δt_{r} is common for all the satellite, δ^i_{ion} depends on the satellite locations. This is an essential feature to distinguish each effect. From Eq. (3.1) and Eq. (3.18), the slant TEC I^i_{slant} is represented by

$$I^i_{\text{slant}} = \Lambda\left(R^i - \rho^i + c\delta t^i_{\text{s}} - \delta^i_{\text{tro}}\right) - \Lambda c\delta t_{\text{r}}. \tag{3.19}$$

We separate the right side of the Eq. (3.19) into two parts; known and unknown parts. The known part and unknown part can be defined as follows

$$\kappa \equiv \Lambda\left(R^i - \rho^i + c\delta t^i_{\text{s}} - \delta^i_{\text{tro}}\right), \tag{3.20}$$

$$\alpha \equiv \Lambda c\delta t_{\text{r}}. \tag{3.21}$$

The ionospheric TEC distribution is generally shown in vertical TEC map. Measured slant TEC, therefore, need to be changed to vertical TEC. Conversion can be done by using a model called slant factor. The conversion is the most important part in the TEC map reconstruction from single frequency GPS data because the effects of slant TEC and receiver clock error on propagation delays should be separated depending on the slant effects. In case the ionosphere is assumed to be a thin layer, the ray path crosses the ionosphere at one point called the ionospheric pierce point (IPP) as shown in Figure 3.4.

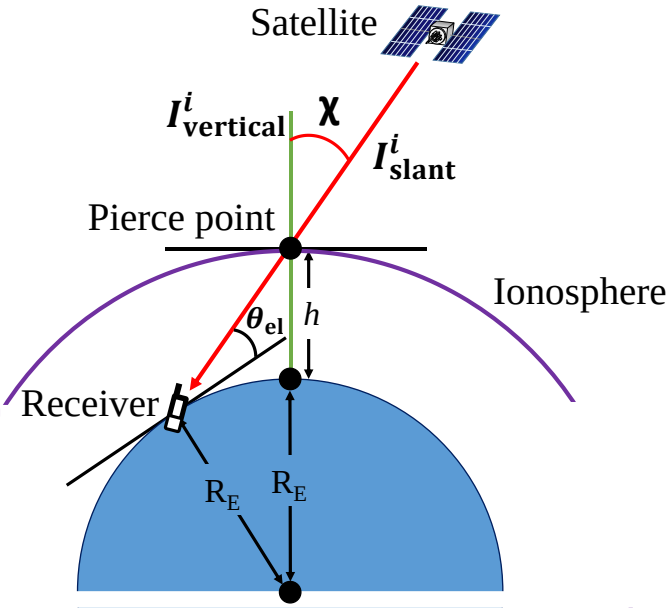

Figure 3.4 Conversion model from slant TEC to vertical TEC in a thin layer assumption for the ionosphere.

In the Klobuchar model [11], the conversion factor from slant TEC I^i_{slant} to vertical TEC I^i_{vertical} is represented as follows;

$$I^i_{\text{slant}} = I^i_{\text{vertical}} \cdot \frac{1}{\cos \chi i}, \tag{3.22}$$

where the angle χ between zenith direction and satellite direction from the IPP can be calculated as follows;

$$\chi i = \sin^{-1}\left(\frac{R_E}{R_E+h}\cos\theta^i_{\text{el}}\right), \tag{3.23}$$

where R_E is Earth radius and h is the altitude of IPP which is assumed to be 350 km. θ_{el}^{i} is elevation angle of the satellite at the receiver location. We adopt this slant effect in this study.

From Eq. (3.19), (3.20), (3.21) and (3.22), vertical TEC can be represented by,

$$I_{\text{vertical}}^{i} = (\kappa - \alpha)\cos\chi \equiv (\kappa - \alpha)\, F, \tag{3.24}$$

where cos χ is defined as a slant factor F.

3.3 Spatial Model of Electron Density and Parameter Estimation

The ionospheric TEC is usually shown in vertical TEC map. In this study, 1st order linear function is used to reconstruct the ionospheric vertical TEC maps with 2-dimensional latitude-longitude gradient. The model covers a small area within several hundred kilometer squares in each dimension and to show variation of electron density distribution. The 1st order vertical TEC distributions are represented as follows;

$$I_{\text{vertical}}^{i} = I_0 + \Delta I_x x + \Delta I_y y, \tag{3.25}$$

where x and y are normalized longitude (local time) and latitude. I_0, ΔI_x, and ΔI_y are vertical TEC at the reference point (135 °E, 36 °N), gradients of vertical TEC for x and y directions. I_0, ΔI_x, and ΔI_y are parameters which should be estimated from measurements. From Eq. (3.24) and Eq. (3.25), we obtained the following relation;

$$I_0 + \Delta I_x x + \Delta I_y y = (\kappa - \alpha)\, F, \tag{3.26}$$

where I_0, ΔI_x, ΔI_y and α are unknown parameters to be solved.

Form the Eq. (3.26), at least four independent equations are required to solve the unknown parameters in the equation, that is, the number of visible satellite from the receiver must be more than four. According to the GPS constellation, this condition is always satisfied. When n number of satellites are visible from the receiver location, the following matrix is obtained,

$$\begin{pmatrix} 1 & x_0 & y_0 & F_1 \\ 1 & x_1 & y_1 & F_2 \\ \vdots & \vdots & \vdots & \vdots \\ 1 & x_n & y_n & F_n \end{pmatrix} \begin{pmatrix} I_0 \\ \Delta I_x \\ \Delta I_y \\ \alpha \end{pmatrix} = \begin{pmatrix} \kappa \cdot F_1 \\ \kappa \cdot F_2 \\ \vdots \\ \kappa \cdot F_n \end{pmatrix}. \tag{3.27}$$

In this equation, (x_i, y_i) denotes location of the pierce point of i^{th} visible satellites and F_i is a slant factor of the i^{th} satellite. When Eq. (3.27) is represented as $\boldsymbol{XI} = \boldsymbol{m}$, unknown vector $\boldsymbol{I}$ can be estimated using linear least square method as follows;

$$\boldsymbol{I} = (\boldsymbol{X}^T\boldsymbol{X})^{-1}\boldsymbol{X}^T\boldsymbol{m}. \tag{3.28}$$

Form this least square method, the unknown parameters in Eq. (3.26) are estimated and those parameters are used in the reconstruction of the vertical TEC map.

CHAPTER 4
APPLICATION TO THE GEONET DATA

The developed method was applied to pseudorange data obtained by the GEONET. Although dual frequency data are available in the GEONET data, only L1 frequency pseudorange data were used for examination of the proposed method.

4.1 Example Analysis for Uchinada Station Data

We show an example result for data obtained at Uchinada station (136°E, 36°N) in Japan on November 10, 2013. From the precise ephemeris at local time of 11:00 am on the day, locations of the pierce points and elevation angle factors are calculated for all visible satellites, which are shown in Figure 4.1. In the figure, horizontal axis is longitudes (local time) and vertical axis is latitudes. The receiver location is shown as blue circle point. The pierce points are shown as red triangle points. The visible satellites ID and its elevation angles are indicated as red numbers with square brackets under the pierce points and black numbers in degree above the pierce points respectively.

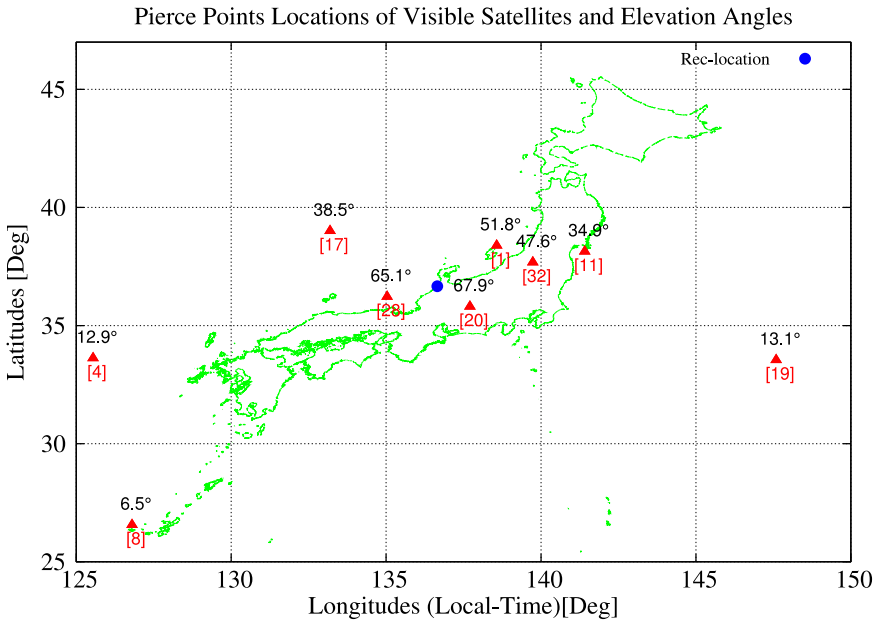

Figure 4.1 Pierce points locations of visible satellites and elevation angles for the example analysis.

We reconstructed the TEC map for this region. Figure 4.2 shows the TEC map at local time of 11 hour in JST (Japan Standard Time) that is 2 hour UT (Universal Time) on Nov. 10. The map was reconstructed from the estimated parameter vector ***I*** in Eq. (3.28). The reconstructed region is from 125°E to 150°E in longitude and from 25°N to 47.5°N in latitude. The color bar at the right side of the figure shows the vertical TEC in TECU. The receiving station is shown as black circle in the figure. The pierce points are shown by blue triangle points. In this period, 9 satellites are visible from the station. Therefore, 9 independent equations were used to estimate four unknown parameters.

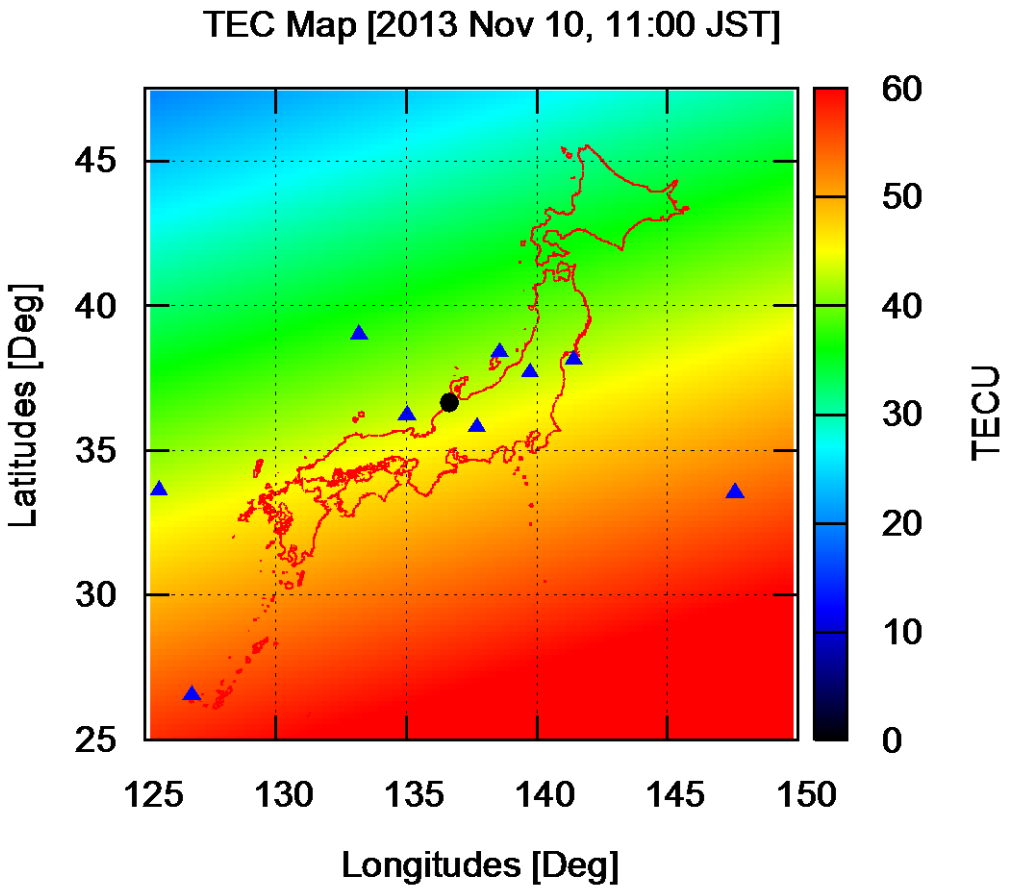

Figure 4.2 Example latitudinal and longitudinal TEC map estimated for the data obtained at Uchinada station in the GEONET.

The result shows the TEC above the receiver location is around 45 TECU and it is decreasing from 50-60 TECU to 30-40 TECU as the location moves from lower to higher latitudes. As for local time variation of the TEC, the maximum value is

generally found in the early afternoon. Since data acquisition time is 11 hour JST and the JST is defined at 135ºE, TEC in the east side of Japan should be larger than the west side. In the result, such longitudinal gradient is clearly found. The estimated values and their variations for latitude and longitude are typical.

We used the global TEC maps derived from dual frequency observations as a comparison of the results from our proposed model. Figure 4.3 shows the longitudinal and latitudinal TEC variation map around Japan provided by the IGS as the GIM on the same period of 11:00 JST on Nov. 10, 2013.

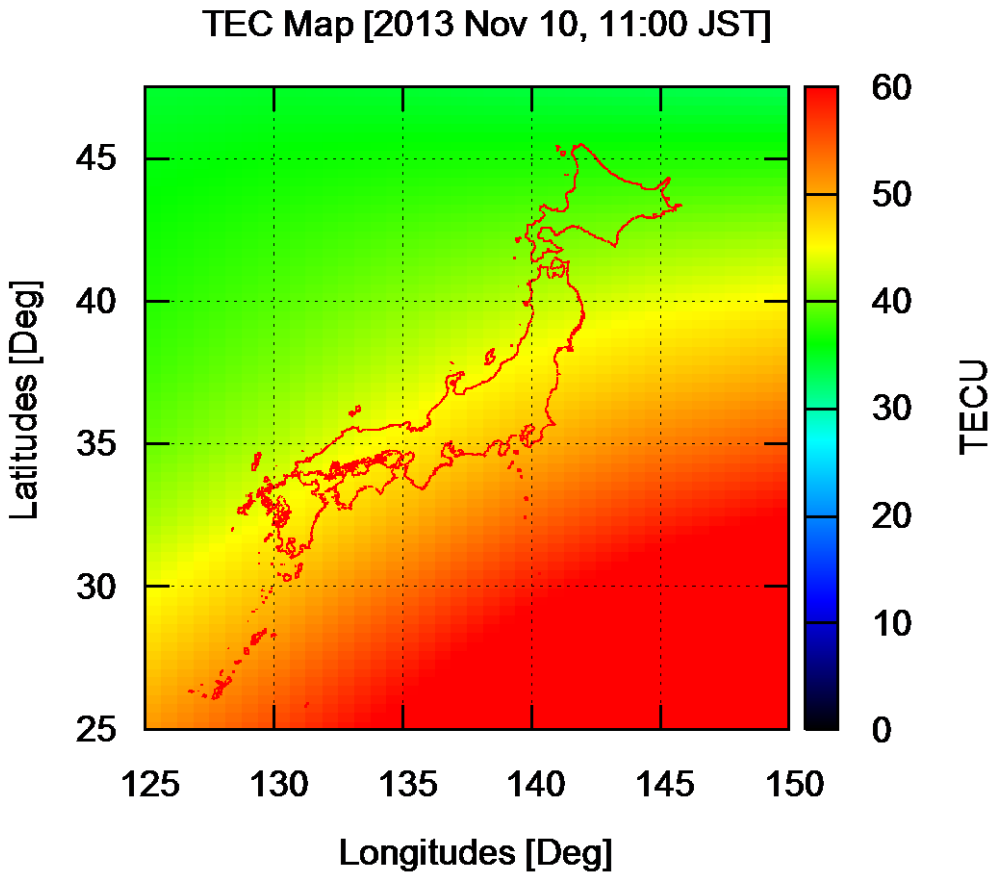

Figure 4.3 Latitudinal and longitudinal TEC map derived by dual frequency measurements provided by the IGS.

In the figure, the latitudinal TEC variation is also higher at lower latitude regions and it is lower at higher latitude regions with TEC values from around 30 TECU to 60 TECU. The result shows the TEC above the receiver location is around 45 TECU and it is decreasing from 50-60 TECU to 30- 40 TECU with moving

locations from lower to higher latitudes. As for local time variation of the TEC, the maximum value is also found in the early afternoon. The TEC values in the morning side at the west part of Japan, are lower than at the east part. By comparison of these two example results, the single frequency result shows almost the same tendency as dual frequency result in latitudinal and longitudinal variations while the TEC values of the single are a few TECU lower than those of the dual at same locations.

4.2 Analysis of One Day Variation

One-day data analysis makes it possible to check the statistical validity of the proposed method to various kinds of TEC variations. We applied the proposed method to the whole data obtained at the Uchinada station on November 10, 2013. The data are provided every 30 seconds and thus, there are 2880 data sets [2]. The parameters I_0, ΔI_x, ΔI_y and α are independently estimated for each data sets. The estimated I_0 is evaluated by comparing with vertical TECs converted from slant TECs that were measured by dual frequency signals at the same times.

Figure 4.4, 4.5 and 4.6 show results of estimated parameters of I_0, ΔI_x, ΔI_y and receiver clock error α and its residual error. In these figures, the horizontal axis shows local time in JST from 9 hour on Nov. 10 to 9 hour on Nov. 11, that is, 0 to 24 hour in UT on Nov. 10. In Figures 4.4 (a), the vertical TECs estimated at the reference point I_0 is represented by a red dotted line and the vertical TEC at each pierce point derived by dual frequency measurement is represented by black line. In dual frequency measurement, satellite and receiver differential code bias (DCB) provided by the IGS and the ENRI, respectively, were used into an account [12]. From this result, both the vertical TECs show around 40 TECU in daytimes from 9 to 15 hour of JST. It is decreasing from 40 TECU to 10 TECU in the evening from 15 to 19 hour. It becomes less than 10 TECU and there is no remarkable variation at night. In the morning, it increases again from 10 TECU to 30 TECU. There seems a good correspondence between I_0 and dual frequency measurement.

The longitudinal and latitudinal gradients of TEC ΔI_x, and ΔI_y are represented by green and by blue lines, respectively, in Figure 4.4 (b). The gradients are defined by TEC variations for 15 degrees in TECU. The longitudinal gradient is plus values before 13 hour. After that, it takes minus values until the next morning. Because longitudinal gradient mainly signifies local time gradient due to the Earth's rotation, it

should take plus values from morning region to the noon. In the afternoon, it should be minus. Thus, the estimated gradient is consistent with the typical local time variation. As a comparison of the results from Figure 4.4 (a) and (b), the local time gradient of vertical TEC I_0 and longitudinal TEC ΔI_x are reasonably same each other. As for latitudinal gradient ΔI_y, it takes minus values except for after midnight. The value is largely fluctuated from around -5 to -40 TECU in the daytime. Since the latitudinal TEC gradient indicates TEC gradients from south to north in the daytime in the northern hemisphere, the result is reasonable.

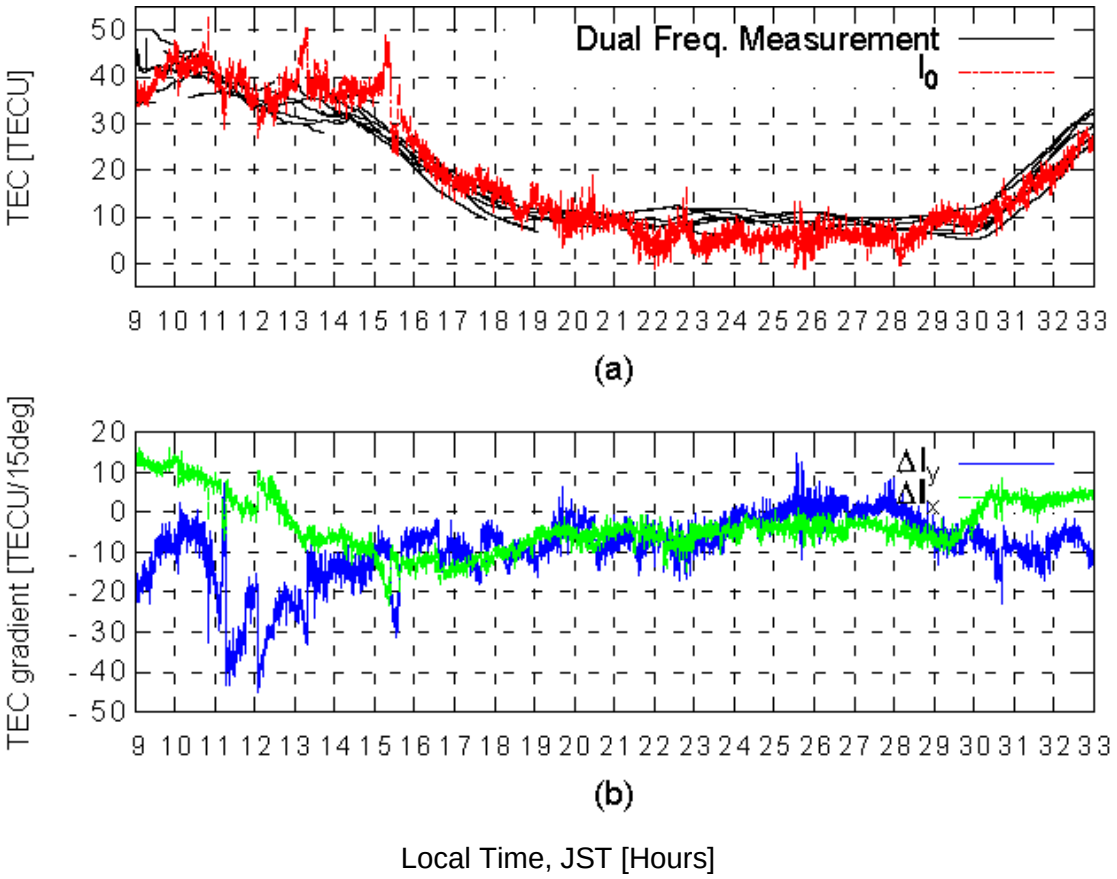

Figure 4.4 (a) Comparison of estimated vertical TEC from single and dual frequency measurements, and (b) estimated longitudinal and latitudinal TEC gradients.

Figure 4.5 shows the estimated receiver clock error α in meter by red dotted line and that derived from the dual frequency measurements by black solid line. Actually, there are two types of GPS receivers; one adjusts its receiver clock error

successively and the other adjusts its clock error after it is accumulated to a certain extent, such as 1 ms. From the absolute values of the receiver clock error in Figure 4.5, it is noted that the receiver of the Uchinada station is former type.

From comparison of the two curves in Figure 4.5, the receiver clock error is well estimated by the proposed method. This means that the assumption of TEC model with 1st order gradients is appropriate during the day. There are small deviations at around local times of 13 hour, 15 hour and 21-26 hours. During these periods, there are also deviations on the estimated TEC in Figure 4.5. Since 1 TECU estimation error corresponds to 16 cm of receiver clock error, the receiver clock error should be estimated with much higher accuracy than its hourly variation to get ionospheric TEC.

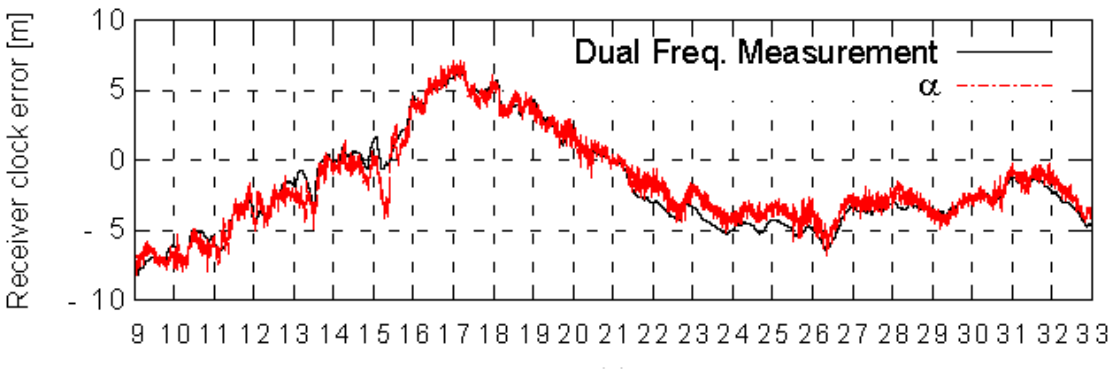

Figure 4.5 Comparison of estimated receiver clock error from single and dual frequency measurements.

Figure 4.6 shows residual error of the least squares method, that is $|\boldsymbol{XI} - \boldsymbol{m}|$. The error is shown in meter. From the result, the fitting error seems around 0.5 m which is equivalent to 3 TECU in average. There are a few peaks during day time in the figure. During these periods, the residual errors are more than 1 meter, which means that the estimated TEC may include errors greater than 6 TECU. The TEC values are, however, large during these periods, and during night time when we have small TEC values, the fitting error is also small.

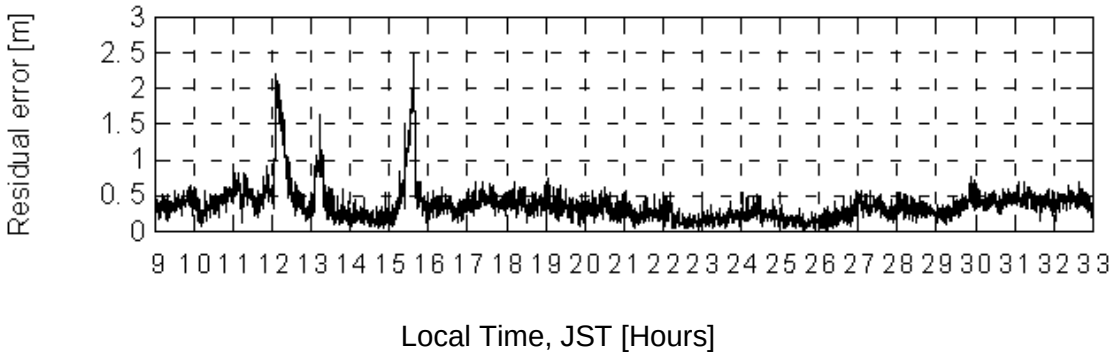

Figure 4.6 Residual error of least square method.

We discuss the TEC errors estimated by the proposed method. Figure 4.7 shows the histogram of the slant TEC errors derived from the estimated parameters to those derived from the dual frequency measurements. The horizontal axis shows the TEC errors in TECU and vertical axis does counts. The average of the TEC error is 0.87 TECU and the standard deviation is 8.52 TECU. There is little artificial bias of the estimated TEC.

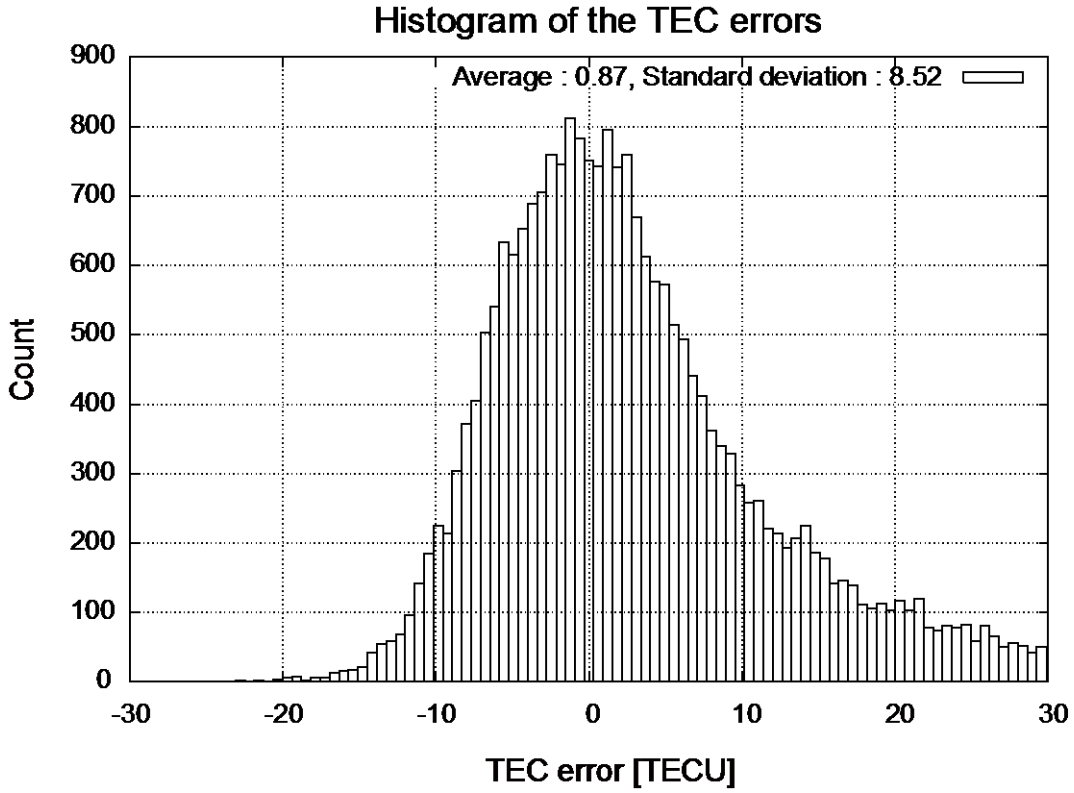

Figure 4.7 Histogram of the TEC errors of the proposed method applied on Uchinada data on 2013 Nov. 10.

4.3 Regional Dependence of TEC Errors

We applied the proposed method to data obtained at other 680 GEONET stations and examined their TEC errors. Figure 4.8 shows spatial distribution of average of the TEC errors. In the figure, the average of TEC estimation error less than -3.16 TECU are shown by red plus points, between -3.16 TECU and 0 are by green crosses, between 0 and +3.16 TECU are as blue stars, and larger than +3.16 TECU are as magenta rectangles points. From the figure, a clear regional dependences of the average of TEC errors is found. In the north parts of Japan, it is occurred negative bias errors and the largest negative bias errors are occurred in east parts of Japan shown as red plus points. However, in the south parts of Japan, positive bias errors are occurred and the largest errors are found in the lowest latitude regions where maximum electron density is existed. As the location moves from north to south, large bias errors appear.

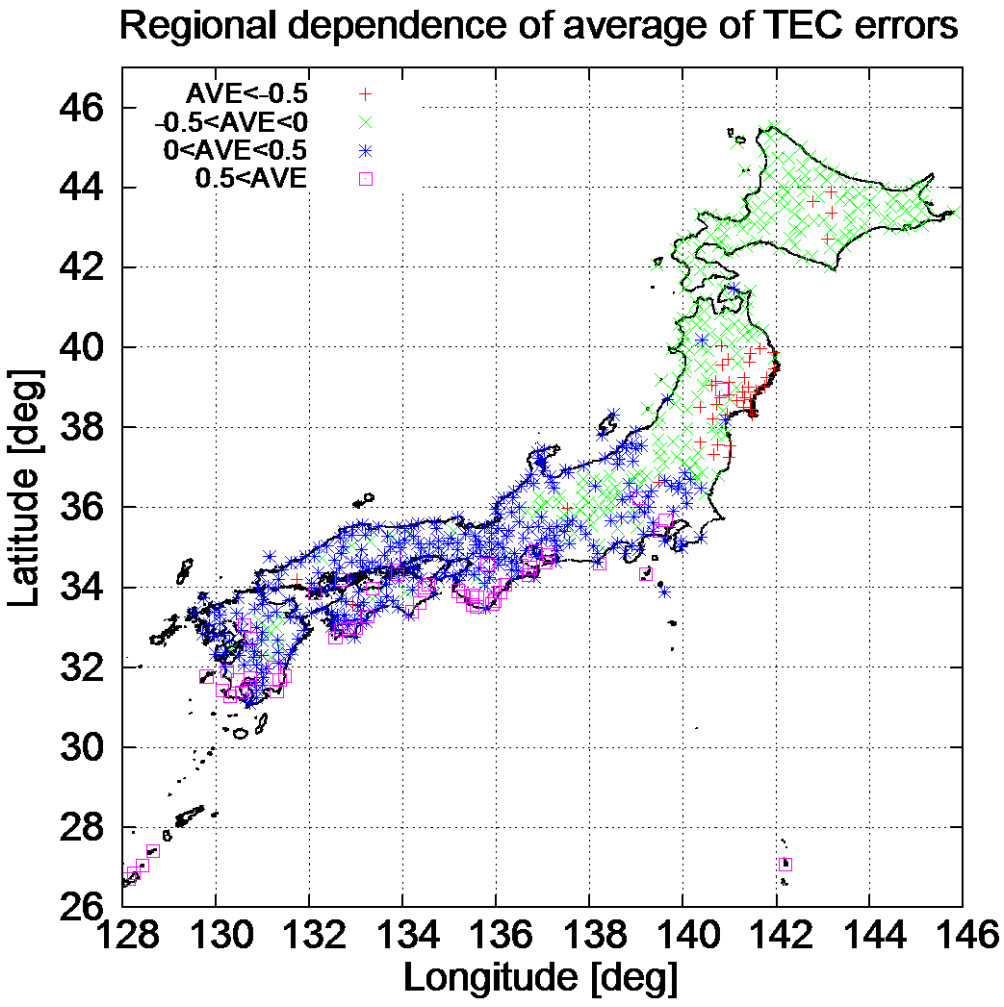

Figure 4.8 Spatial distribution of average of the TEC errors.

We also examined the regional dependences of the standard deviation of the TEC errors. The result is shown in Figure 4.9. In the figure, the standard deviation less than 9.2 are shown by red plus points, between 9.2 and 12.3 are by green crosses, between 12.3 and 18.5 are by blue stars, and larger than 18.5 are by magenta rectangles points. The largest standard deviation is found at around (141°E, 38°N) and it becomes smaller as the location moves away from there.

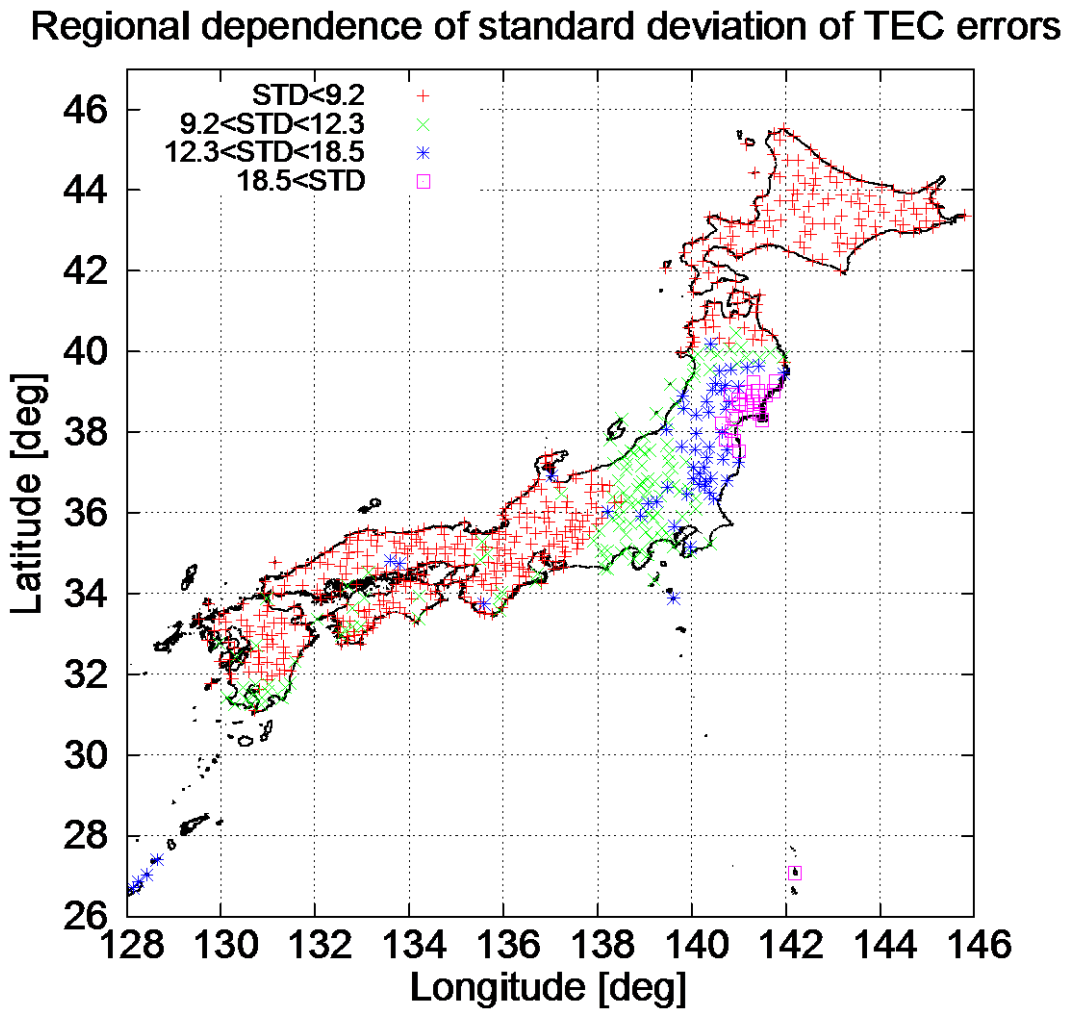

Figure 4.9 Spatial distribution of standard deviation of the TEC errors.

There is no regional dependence of performance of the receivers in GEONET, and thus the large standard deviations found at (141°E, 38°N) is due to other effects. It is near the Sendai regions in Japan. On that region, there was big earthquake in 2011 as a center at that regions. The locations of GPS receivers were known to be moved. It is, then, considered that there are errors in the given receiver locations. In the proposed method, the receiver location should be updated.

It is also found that the accuracy of the proposed method depends deeply on the assumption of the spatial distribution of the TEC. In the method, we assume that the TEC variation is represented by 1^{st} order gradient for both latitude and longitude. From the average distribution, however, when the receiver is located at lower latitudes where a large latitudinal TEC gradient exists in a typical daytime, accuracy of the TEC estimation becomes worse. This result implies that the latitudinal assumption is not appropriate in such regions. To apply the method to the data obtained at low latitude regions near equator, TEC variations are much complex due to various phenomena, such as plasma bubble, and higher order function or more appropriate model should be required.

The location of pierce points and number of pierce points are important in the method to estimate accurate TEC distribution. Multiple receiver observations are, therefore, efficient. In such observations, the number of estimated parameters should be increased while we can extend the estimation method to such situation easily.

CHAPTER 5
CONCLUSIONS

In this paper, an estimation method of ionospheric TEC distribution from GPS signal is proposed. A significant point of the method is that it only uses single frequency measurements while the TEC observation is generally realized by dual frequency measurements because only the ionospheric delay among various errors in the GPS observables has frequency dependence. Since the cost of dual frequency receivers are much higher than single ones, it becomes easy, by this method, to construct TEC observation networks at low costs where the GPS networks are not yet installed.

In the developed method, the TEC distribution in a small area within a several hundred kilometers squares is assumed to be represented by a first order gradient model for latitude and longitude. The unknown parameters for ionospheric TEC distribution model and receiver clock errors are estimated by a least squares method. We evaluated the developed method by comparing the results with those from the dual frequency measurements. The evaluation was conducted using GPS data obtained at GEONET stations. As a result, the accuracy of the model is approximately less than 10 TECU in RMS. The first order assumption sometimes causes large TEC errors when the TEC distributions have unexpected structures. TEC gradients from low to mid latitudes in a daytime may not be represented by the model. To solve this problem, higher order formula, such as second order polynomial functions, is considered to be effective. When we adopt higher order functions, the number of parameters to be solved increases. Using data from multiple receivers, we can increase several independent equations for one receiver while we should estimate a receiver clock error as an additional parameter for each receiver. This modification remains to be solved in the future study.

REFERENCES

[1] D. Bilitza, D. Altadill, Y. Zhang, C. Mertens, V. Truhlik, P. Richards, L. A. McKinnell, and B. Reinisch, The International Reference Ionosphere 2012 – a model of international collaboration, *J. Space Weather Space Clim.*, 4, A07, 1-12, 2014.

[2] The GEONET Group, Geographical Survey Institute, GEONET (GPS Earth Observation Network System) and its Prospect, *J. Geodetic Society of Japan*, 50, 2, 53-65, 2004.

[3] J. Feltens, The International GPS Service (IGS) Ionosphere Working Group, *Adv Space Res*., 31(3), 635–644, 2003.

[4] M. Hernández-Pajares, J. M. Juan, J. Sanz, R. Orus, A. Garcia-Rigo, J. Feltens, A. Komjathy, S. C. Schaer, and A. Krankowski, The IGS VTEC maps: a reliable source of ionospheric information since 1998, *J. Geodesy*, 83, 3, 263-275, 2009.

[5] S. Schaer, W. Gurtner, and J. Feltens, *IONEX: The IONosphere Map Exchange Format Version 1 (Proposal, February 1997)*, Astronomical Institute, University of Berne, 1998.

[6] B. W. Parkinson and J. J. Spilker Jr Eds., Global Positioning System: Theory and Applications, I, II, *American Institute of Aeronautics and Astronautics*, 1997.

[7] J. G. Grimes, Global Positioning System Standard Positioning Service Performance Standard, *U.S. Department of Defense*, 2008.

[8] P. Misra, P. Enge Eds., Global Positioning System: Signals, Measurements, and Performance. Second Edition, *Ganga-Jamuna Press*, 2011.

[9] P. R. Spofford, and B. W. Remondi, The National Geodetic Survey Standard GPS Format SP3. (SP3-a format), 1994, available from the IGS website: https://igscb.jpl.nasa.gov/igscb/data/format/sp3_docu.txt

[10] M. J. Dunn, Global Positioning Systems Directorate Systems Engineering and Integration, Interface Specification, Navstar GPS Space Segment/Navigation User Interface, IS-GPS-200H, *U.S. Department of Defense*, 2013.

[11] J. A. Klobuchar, Ionospheric time-delay algorithm for single-frequency GPS users, *IEEE Trans. on Aero. and Elec. Sys.*, AES-23, 3, 1987.

[12] S. Schaer, Overview of GNSS biases, *IGS Workshop on GNSS Biases*, University of Bern, 2012, available from the CODE ftp site: ftp://ftp.unibe.ch/aiub/CODE/